Biophysical Chemistry 185 (2014) 79–87

Contents lists available at ScienceDirect

Biophysical Chemistry

journal homepage: http://www.elsevier.com/locate/biophyschem

Reduction of the C191-C220 disulfide of α-chymotrypsinogen A reduces nucleation barriers for aggregation

William F. Weiss IV [a,1], Aming Zhang [b], Magdalena I. Ivanova [c,3], Erinc Sahin [a,2], Jacob L. Jordan [b], Erik J. Fernandez [b], Christopher J. Roberts [a,*]

[a] Department of Chemical and Biomolecular Engineering, University of Delaware, Newark, DE 19716, United States
[b] Department of Chemical Engineering, University of Virginia, Charlottesville, VA 22904, United States
[c] Molecular Biology Institute, University of California, Los Angeles, CA 90095, United States

HIGHLIGHTS

- Aggregation of chymotrypsinogen results in amyloid polymers at acidic pH.
- Removal of the C191-C220 disulfide does not change the measurable secondary or tertiary structure by CD or fluorescence.
- Removing the C191-C220 disulfide lowers the nucleation barrier, and shifts the nucleus size from an oligomer to a monomer.

GRAPHICAL ABSTRACT

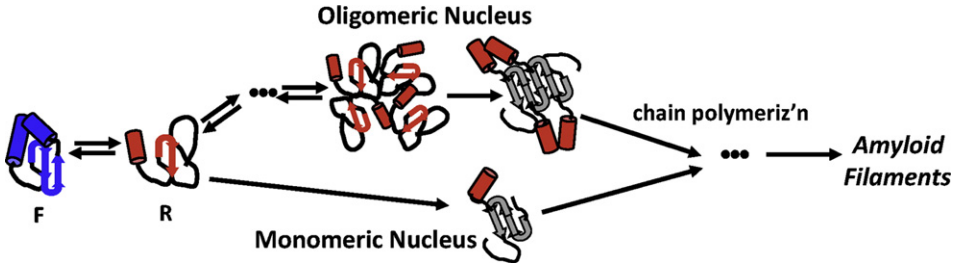

ARTICLE INFO

Article history:
Received 2 October 2013
Received in revised form 5 November 2013
Accepted 14 November 2013
Available online 28 November 2013

Keywords:
Protein unfolding
Protein aggregation
Disulfide bond
Aggregate structure

ABSTRACT

Proper disulfide formation can be essential for the conformational stability of natively folded proteins. For proteins that must unfold in order to aggregate, disruption of native disulfides may therefore promote aggregation. This study characterizes differences in the aggregation process for wild-type (WT) α-chymostrypsinogen A (aCgn) and the same molecule with one of its native disulfides (C191-C220) reduced to free thiols (aCgnSH) at acidic pH, where WT aCgn forms semi-flexible amyloid polymers. Loss of the disulfide leads to no discernable differences in folded monomer secondary or tertiary structure based on circular dichroism (CD) or intrinsic fluorescence (FL), and causes a small decrease in the free energy change upon unfolding. After unfolding-mediated aggregation, the resulting amyloid morphology and structure are similar or indistinguishable for aCgn and aCgnSH by CD, FL, ThT binding, multi-angle laser light scattering, and transmission electron microscopy. Aggregates of aCgn and aCgnSH are also able to cross-seed with monomers of the other species. However, aggregates of aCgnSH are more resistive than aCgn aggregates to urea-mediated dissociation, suggesting some degree of structural differences in the aggregated species that was not resolvable in detail without higher resolution methods. Mechanistic analyses of aggregation kinetics indicate that the initiation or nucleation of new aggregates from aCgnSH involves a mono-molecular rate limiting step, possibly the unfolding step. In contrast, that for aCgn involves an oligomeric intermediate, suggesting native disulfide linkages help to hinder non-native protein aggregation by providing conformational barriers to key nucleation event(s).

* Corresponding author. Tel.: +1 302 831 0838; fax: +1 302 831 1048.
E-mail address: cjr@udel.edu (C.J. Roberts).
[1] Present Address: Biopharmaceutical Research and Development, Eli Lilly and Co., Indianapolis, IN 46285.
[2] Present Address: Drug Product Science and Technology, Bristol-Myers Squibb, New Brunswick, NJ 08903.
[3] Present Address: 4158 BSRB, University of Michigan, Ann Arbor, MI 48109, United States.

0301-4622/$ – see front matter
http://dx.doi.org/10.1016/j.bpc.2013.11.005

1. Introduction

For natively folded proteins, nonnative aggregation denotes the process by which protein monomers assemble into soluble or insoluble aggregates in which the constituent monomers have lost a significant degree of native tertiary and/or secondary structure. The constituent monomers are joined together via covalent or non-covalent interactions, and are often enriched in intra- or inter-molecular β-sheet — with amyloid aggregates as a familiar example [1–5]. The early stages of nonnative aggregation typically involve monomers in partially or fully unfolded states, and therefore protein conformational stability (i.e., unfolding free energy, ΔG_{unf}) often influences overall rates of monomer loss if aggregation is slow compared to folding-unfolding kinetics. This follows because the rate-limiting step(s) for aggregation are "downstream" from unfolding, and therefore the thermodynamics of unfolding, rather than unfolding kinetics, control the concentration or population of "reactive" partially or fully unfolded monomers that are available to nucleate new aggregates or add to existing aggregates [2,5].

The control and prevention of nonnative aggregation remains an ongoing challenge in the biopharmaceutical industry due to concerns ranging from pharmaceutical elegance to efficacy and safety [5–9]. Likewise, a number of debilitating diseases have been linked to nonnative aggregation [4,10,11]. In some cases, chemical changes in the monomer structure due to oxidation or deamidation are thought to promote subsequent aggregation [12,13], but in general there remain outstanding questions regarding the mechanism(s) of, and possible strategies to control this process [13].

Changes in disulfide patterns in folded proteins, and/or cleavage of native disulfides are a concern during recombinant protein refolding, as well as upon long-term storage of protein pharmaceuticals [4]. Loss of native disulfides may be anticipated to result in lower values for the free energy of unfolding (ΔG_{unf}), but it is not clear, in general, whether this will translate to changes in aggregation rate(s) and/or mechanisms. In this context, one approach to influence nonnative aggregation rates is to alter the protein primary sequence via site-directed mutagenesis so as to change ΔG_{unf} [14,15]. For some amyloidogenic proteins, mutations that lead to increased/decreased conformational stability result in lower/higher rates of aggregation [16], in keeping with the qualitative arguments above.

The present study focuses on α-chymotrypsinogen A (aCgn) as a model system to assess the effects on aggregation rates and mechanism(s) due to the loss of a single native disulfide bond. aCgn is a natively monomeric, 25.7 kDa protein that readily forms soluble, amyloid polymers at elevated temperatures under acidic conditions at low ionic strength [17–20]. Wild-type aCgn has five native disulfide bonds (between residues 1-122, 42-58, 136-201, 168-182, and 191-220) and no free cysteines. It unfolds reversibly to a molten-globule state if aggregation can be suppressed by working at low protein concentration [19,20]. Aggregate formation for aCgn proceeds primarily through an oligomeric nucleus with growth dominated by monomer addition so long as one avoids higher pH and salt conditions where aggregate–aggregate condensation is kinetically relevant [18–21]. Aggregation rates of aCgn are strongly correlated with the unfolding free energy [19,21]. Therefore, as a basis of the present work, it was hypothesized that removal of one or more native disulfide bonds may not only significantly accelerate aggregation rates by reducing ΔG_{unf}, but also might alter the aggregate mechanism itself if it altered the nature of the nuclei and/or resulting structure of the aggregates.

In this report, a number of experimental techniques were used to study the effects of removing a native disulfide bond on the aggregate structure/morphology, the kinetics and oligomerization state of intermediates in the aggregation pathway, and the unfolding thermodynamics of aCgn. Hydrogen-deuterium exchange with mass spectrometry (HDX-MS) was used to identify the location of the reduced disulfide bond and to confirm that, on average, only a single reduced S – S bond existed. Multi-angle light scattering (MALS), transmission electron microscopy (TEM), fiber X-ray diffraction, and ThT binding were used to characterize aggregate morphology and amyloid structure. Circular dichroism (CD) spectroscopy and intrinsic fluorescence were used to compare secondary and tertiary structure, respectively, of native and chemically-unfolded monomers, and of aggregated aCgn and aCgnSH. Equilibrium urea unfolding/refolding experiments provided a comparison of ΔG_{unf} for monomeric aCgn and aCgnSH. Mechanistic analysis of the kinetics of monomer loss and changes in aggregate molecular weight, as a function of initial protein concentration (c_0), were used to infer differences and similarities in the nucleation and growth mechanisms for aCgn and aCgnSH, similar to that done previously for aCgn [17,19,22,23].

2. Materials and methods

aCgn (lyophilized powder, 5× crystallized, lot number 37J9779) was purchased from Worthington Biochemical Corp. (Milford, MA) and used without further purification. Tris(2-carboxyethyl)phosphine hydrochloride (TCEP), citric acid monohydrate, sodium hydroxide, sodium phosphate, and ethylenediaminetetraacetic acid (EDTA) were purchased from Thermo Fisher Scientific (Waltham, MA). 5-5′-dithiobis(2-nitrobenzoic acid) (DTNB) was purchased from Sigma-Aldrich (St. Louis, MO). Ultra pure urea and thioflavine T (ThT) were purchased from MP Biomedicals, Inc. (Solon, OH). Distilled, deionized water from a Millipore (Billerica, MA) Milli-Q filtration system with a Quantum EX ultrapure Organex cartridge was used in the preparation of all buffers, protein solutions, and mobile phases. aCgn solutions were prepared in 10 mM citrate buffer pH 3.5 as described previously [20].

2.1. Preparation of partially-reduced aCgn (aCgnSH)

10 mM citrate, 20 mM TCEP pH 3.5 buffer (reducing buffer) was freshly prepared and refrigerated (4–8 °C) overnight (approximately 8 h). Lyophilized aCgn powder was added to an aliquot of cold reducing buffer, resulting in a protein concentration of approximately 10 mg/mL (398 μM). The resulting solution was then incubated under refrigerated conditions for 2.5 h.

At the end of the incubation period the partially-reduced aCgn was separated from the TCEP using an ÄKTA Explorer liquid chromatography system equipped with a P-950 sample pump, UV-900 multi-wavelength detector, and Frac-950 fraction collector (GE Healthcare, Piscataway, NJ). A HiPrep 26/10 desalting column (GE Healthcare) was equilibrated with 5 column volumes (~265 mL) of 10 mM citrate pH 3.5 mobile phase before loading a 10 mL bolus of partially-reduced aCgn solution at 9 mL/min using the P-950 sample pump. The sample was eluted isocratically at 9 mL/min and an 8 mL protein fraction was collected. Additional details are included in Supporting information.

Ellman's assay was used to determine the number of reduced disulfide bonds in the resulting partially-reduced aCgn sample [24–26]. Partially reduced aCgn solution (nominally 40–60 mg) was combined with 2.8 g of 100 mM sodium phosphate, 1 mM EDTA pH 7.3 buffer in a 1 × 1 cm cuvette (Hellma USA, Plainview, NY). The resulting solution was equilibrated at 20.0 ± 0.1 °C in a TLC 40 single cell holder with a TLC 125 Peltier controller (Quantum Northwest, Liberty Lake, WA) for 10 min before measuring the absorbance at 280 nm with an Agilent Technologies (Santa Clara, CA) 8453 spectrophotometer and converting to concentration using a molar extinction coefficient of $5.14 \times 10^4\ M^{-1}\ cm^{-1}$ [27]. The concentration of free thiol groups was then determined by adding 150 μL of a solution containing 3 mM DTNB, 100 mM sodium phosphate, 1 mM EDTA pH 7.3 to the cuvette, recording the absorbance at 412 nm, and converting to concentration using a molar extinction coefficient of $1.415 \times 10^4\ M^{-1}\ cm^{-1}$ [25]. The number of reduced disulfide bonds was calculated as the average of three measurements. Additional details are included in Supporting information.

2.2. Mass spectrometry for reduced disulfide bond identification and isotope exchange

The reduced disulfide bond in aCgnSH was identified by means of chemical modification coupled with MS/MS mass spectrometry. Partially reduced aCgn (50 μL) was first mixed with the same volume of 50 mM Tris buffer to adjust the solution pH to 8. Free thiol carboxyamidation was performed by adding 10 μL 200 mM iodoacetamide stock solution, followed by reaction for 45 min in the dark. The modified aCgnSH was subjected to trypsin digestion at 37 °C for 6 h at a substrate:enzyme ratio of 10:1. The enzymatic digestion was quenched by a pH shift to 2.7 using 50% (v/v) acetic acid solution. The fully digested aCgnSH was finally treated with 100 mM TCEP for 2 min to reduce all the other disulfide bonds before injecting to an ESI mass spectrometer (Thermo Finnigan LTQ, Thermo Electron Corporation, San Jose, CA) for the MS/MS peptide sequencing identification. Additional details are provided in Supporting information.

2.3. Size exclusion chromatography with inline multi-angle laser light scattering (SEC-MALS)

Analytical size exclusion chromatography was performed, and monomer concentrations quantified, with a Waters (Milford, MA) Alliance 2695 separations module with a 2996 photodiode array detector (DAD) and Protein-Pak 7.8 × 300 mm size exclusion chromatography column, as described previously [20]. Fractionated samples were routed to a DAWN HELEOS II multi-angle light scattering detector (Wyatt Technology Co., Santa Clara, CA) and then to a Optilab rEX (Wyatt) differential refractive index (RI) detector. The MALS unit was equipped with 16 detectors between 32° and 147°. Raw data signals from the DAD, MALS, and RI detector were processed using Astra V® software (Wyatt).

Analysis of static light scattering data from SEC-MALS is described in detail elsewhere [17]. Briefly, weight-average molecular weight (M_w) and radius of gyration (R_g) were determined from the Zimm equation,

$$\frac{Kc}{R_{ex}} = \frac{1}{M_w}\left(1 + \frac{q^2 R_g^2}{3}\right) + 2B_{22}c \tag{1}$$

where K is the optical constant, c is the mass concentration of protein, R_{ex} is the excess Rayleigh ratio, q is the magnitude of the scattering vector, and B_{22} is the second osmotic virial coefficient. In all cases reported here, the concentration of protein is sufficiently low and the magnitude of B_{22} sufficiently small that the term $2B_{22}c$ can be neglected [17].

Eq. (1) was applied to light scattering data averaged over small "slices" of the chromatographic peak. The weight-average molecular weight (M_w), and radius of gyration (R_g) for the peak were then calculated as [17,28]

$$M_w = \sum_{i=1}^{i*}\left[c_i (M_i)_w\right] / \sum_{i=1}^{i*} c_i \tag{2a}$$

$$R_g = \left[\sum_{i=1}^{i*}\left(c_i M_i R_{g,i}^2\right) / \sum_{i=1}^{i*}(c_i M_i)\right]^{-1/2} \tag{2b}$$

where c_i, M_i, and $R_{g,i}^2$ are the values for the ith slice and where the summation runs from 1 to i^*, the total number of slices. The value of M_w from this procedure is formally identical to the value from traditional batch light scattering, provided there is not significant loss of protein mass due to adsorption to the column [17,28]. Total chromatogram areas were monitored to assure negligible adsorption to the column for all reported results.

2.4. Circular dichroism (CD)

Equilibrium, isothermal far-UV circular dichroism measurements were performed using a Jasco (Easton, MD) J-810 spectropolarimeter and a Jasco PTC-424S Peltier temperature controller at 20 °C ± 0.2 °C. Spectra were recorded from 260 to 200 nm for aggregated samples (protein mass fraction as aggregate = 0.95 ± 0.02) and native monomeric samples in the absence of urea, and from 260 to 215 nm for monomeric samples containing 6 M urea. In all cases, spectra were recorded at a scanning rate of 50 nm/min at a total protein concentration of 0.2 mg/mL in a 1 × 0 mm Hellma (Plainview, NY) quartz cuvette. Twelve spectra were recorded and averaged prior to subtraction of a buffer baseline. The mean residue ellipticity ($[\theta]$ [=] deg cm^2 dmol^{-1}) was calculated as $[\theta] = \theta M_0 / 10 c_0 d n_r$ where θ is the average ellipticity in mdeg, M_0 is the molecular weight of the protein monomer in g/mol, c_0 is the mass concentration of the protein in mg/mL, d is the path length of the cuvette in cm, and n_r is the number of amino acid residues in the monomer.

2.5. Electron microscopy

Negatively stained specimens for transmission electron microscopy (TEM) were prepared by applying 5 μL of sample on hydrophilic 400 mesh carbon-coated formvar support films mounted on copper grids (Ted Pella, Inc.). The samples were allowed to adhere for 3 min, rinsed twice with distilled water and stained for 1 min with 1% uranyl acetate (Ted Pella, Inc.). Grids were examined in a JEM1200-EX (JOEL) microscope.

2.6. Intrinsic fluorescence

Intrinsic fluorescence measurements were performed with a PC1 spectrofluorimeter (ISS, Champaign, IL) equipped with a TURRET 400 4-position sample holder and TC 125 Peltier temperature controller (Quantum Northwest). The excitation wavelength was 280 nm and emission intensities were recorded from 300 to 450 nm in 1 nm increments. Three spectra were recorded and averaged prior to subtraction of the buffer baseline. Excitation and emission slit widths were 1 and 2 nm, respectively. Excitation and emission polarization angles were 90° and 0°, respectively. All samples were contained in 3 × 10 mm quartz cuvettes (Hellma).

Spectra were recorded for native monomer in the absence of urea, unfolded monomer in 6 M urea, and aggregated samples (mass fraction of aggregate = 0.95 ± 0.02 by SEC) of aCgn and aCgnSH, respectively, at a protein concentration of 0.2 mg/mL.

2.7. Chemical unfolding/refolding

Chemical unfolding/refolding measurements were carried out at 20 and 30 °C ± 0.2 °C. Unfolding samples were prepared by gravimetrically combining aCgnSH stock solution (nominally 9.3 mg/mL in 10 mM citrate pH 3.5 buffer), urea stock solution (8.5 M urea, 10 mM citrate pH 3.5) and citrate buffer (10 mM citrate pH 3.5) to yield samples containing 0–6 M urea and 0.2 mg/mL aCgnSH. Urea molarity was calculated based on measured molality and literature values for solution density as a function of urea concentration [29]. Refolding samples were prepared by gravimetrically combining aCgnSH stock solution with urea stock solution to yield starting samples in 6 M urea. This solution was then equilibrated at the temperature of interest for 20 min before being combined with urea stock solution and citrate buffer by mass to yield samples containing 0.5–6 M urea and 0.2 mg/mL aCgnSH. Appropriate equilibration times were determined by collecting emission spectra as a function of time for selected unfolding and refolding samples spanning the range of temperatures and urea concentrations (20–180 min, data not shown). After equilibration, 3 successive emission spectra were recorded and averaged prior to subtraction of

corresponding buffer spectra. Spectral center-of-mass (COM) was calculated as described previously [19].

2.8. Aggregation kinetics and analysis of mechanisms

Nonnative aggregation kinetics for aCgnSH were accelerated by incubating monomeric protein solutions at elevated temperature ($T \geq 50$ °C). Size exclusion chromatography was used to monitor monomer concentration as a function of time. Representative chromatograms are shown in Supporting information. All detectable aggregates co-eluted in the void volume, and were baseline resolved from the monomer, consistent with results reported earlier for the unreduced molecule [17–20]. Isothermal monomer loss kinetics were measured at 50 °C for a range of initial monomer concentrations (c_0), and at $c_0 = 1.2$ mg mL^{-1} for a series of different temperatures. The kinetics of monomer loss, when combined with the analysis of aggregate molecular weights, provide a means to assess qualitative and quantitative aspects of the aggregation mechanism using the procedure described below and used previously with aCgn [18,20].

The resulting kinetic traces were each fit using a nonlinear least squares algorithm implemented in MATLAB® (Natworks). Monomer loss versus time was fit to the equation, $dm/dt = -k_{obs}m^{\nu}$, where m is the fractional monomer concentration, defined as the concentration of monomer (c) divided by its initial value (c_0); t is the incubation time; k_{obs} is the observed or effective rate coefficient in units of inverse time; and ν is an apparent reaction order that was permitted to take non-integer values for the purpose of fitting and interpolating $m(t)$ data [20]. For scaling purposes, the kinetic half-life (t_{50}) was defined as the time at which the monomer concentration decayed to half of its initial value ($m(t_{50}) = 0.5$). Values of t_{50} were calculated as $t_{50} = (2^{\nu-1} - 1)/[(\nu - 1)k_{obs}]$, with $\nu \neq 1$. The results below do not change substantially if one instead simply interpolates the raw $m(t)$ data to identify t_{50} from $m(t_{50}) = 0.5$.

The subsequent analysis based on the Lumry–Eyring Nucleated Polymerization (LENP) model [22] was used for comparison with previous work with aCgn at the same solvent conditions [17–20]. The limiting values of the aggregate M_w (i.e., extrapolated to $m \to 0$) were combined with the t_{50} values to infer the values for the characteristic timescale (inverse rate coefficient) for initiation/nucleation of new aggregates (τ_n) and the characteristic timescale for growth by monomer addition (τ_g) — see also Results. These values follow from the following relationships [20]

$$\tau_n = (M_w/M_0)_{m\to 0} k_{obs}^{-1} \sim c_0^{1-x} \tag{4a}$$

$$\tau_g = (M_w/M_0)_{m\to 0}^{-1} k_{obs}^{-1} \sim c_0^{-\delta} \tag{4b}$$

which hold when aggregate growth is predominantly via chain-polymerization. In that case, M_w is linear in (1-m) once m is significantly less than 1, and the value of the reduced weight-average molecular weight (M_w/M_0) in the limit of monomer fraction (m) approaching zero scales with the initial protein concentration (c_0) as $(M_w/M_0)_{m\to 0} \sim c_0^{(1+\delta-x)/2}$, where δ is the number of monomers needed from a kinetic standpoint for each growth step, x is the stoichiometry of the nucleus, and M_0 is the monomer molecular weight [22]. This analysis gives the number of proteins (x) involved in the rate-limiting step for nucleation, and the number of monomers (δ) per growth step. For reference, these values are $x = 3$–4 and $\delta = 1$ for aCgn under the same solvent conditions in previous work [18–20].

3. Results

A recombinant form of aCgn is not presently available; therefore, disulfide reduction was accomplished chemically. Based on preliminary studies it was determined that the singly-reduced molecule (aCgnSH) could be isolated as a stable monomer at ambient or colder conditions; however, reduction of additional disulfides resulted in spontaneous creation of aggregates that were not recoverable as monomers. The results in Supplementary Material show that aCgnSH has an average of two free cysteines, indicating a single disulfide is reduced per monomer.

Isolating an initially monomeric product was necessary to enable an unambiguous interpretation of experimental structural, dynamic, and thermodynamic information for comparison with the wild-type system. In studies of this type free thiols are often chemically modified or capped to negate the possibility of disulfide shuffling or the formation of intermolecular disulfide bonds. At low pH, however, the intrinsic reactivity of free thiols is low [30,31] and chemical modifications can complicate the interpretation of thermodynamic data. For example, one report noted ~2 kcal mol^{-1} difference in measured values for the free energy of unfolding based on the choice of capping reagent [32]. For these reasons, and the fact that available data for comparison with aCgn are at pH 3.5, the free thiols were left unmodified.

3.1. Identification of the reduced disulfide bond in aCgnSH

The reduced disulfide bond in aCgnSH was identified by carboxyamidating the free thiols, followed by MS/MS peptide sequencing. Intact, carboxyamidated aCgn was first analyzed to determine the number of chemical modifications (i.e. the free thiol number). Fig. S1A (in Supporting information) shows the mass spectra of aCgn before and after modification with a charge distribution. The mass increase calculated from the +14 charge state (the inset) was 114.6 Da. Because carboxyamidation at one free thiol will increase the molecule weight by 57 Da, the observed mass shift for intact aCgn molecule indicated two free thiols were present in the aCgnSH species here, derived from one broken disulfide bond.

To identify the reduced disulfide bond, aCgnSH was digested with trypsin. A series of polypeptides containing Cys were assigned and examined for carboxyamidation modification of free thiols. The resulting mass spectra indicate the reduction of disulfide bond C191-C220, while the spectra from the other four native S–S containing peptides did not indicate carboxyamidation (data not shown). In Fig. S1B (Supporting information), the measured mass of assigned peptide 178–191 increased by 57 Da, the expected mass difference for one thiol carboxyamidation. Peptide sequencing based on the MS/MS spectrum in Fig. S1C established the reduced Cys was Cys 191. Reduction of C191-C220 is also consistent with other reports [33]. As noted below, aggregates of aCgnSH were not reversible in concentrated urea or guanidine HCl, and as such were not amenable to hydrogen-deuterium exchange with MS methods for ascertaining differences between local structure/exposure for aggregates of aCgn and aCgnSH.

3.2. Aggregation kinetics and LENP analysis

Fig. 1 shows m versus reduced time (t/t_{50}) for aCgnSH at 50 °C for values of c_0 spanning nearly an order of magnitude from 0.6 to 4.0 mg/mL, and at $c_0 = 1.2$ mg mL^{-1} for temperatures from 51 °C to 54 °C. The data for different c_0 values at 50 °C (panel A) fall on a common curve within statistical uncertainty, as found previously for aCgn [19]. Similar behavior is observed as a function of temperature with fixed $c_0 = 1.2$. Table S1 (Supplementary Material) summarizes the numerical results of the nonlinear least squares fitting of the isothermal monomer loss kinetics.

Fig. 2 shows M_w/M_0 values for aCgnSH aggregates obtained from SEC-MALS measurements versus extent of reaction ($1 - m$) for a range of c_0 values from 0.6 to 4.0 mg mL^{-1}. The limiting $(M_w/M_0)_{m\to 0}$ values for aCgnSH aggregates were calculated from a linear extrapolation of the final five data points for a given c_0 value, as shown in Fig. 2. The linear relationship between values of M_w/M_0 and $1 - m$ when $t \geq t_{50}$ is an important experimental signature indicative of aggregate

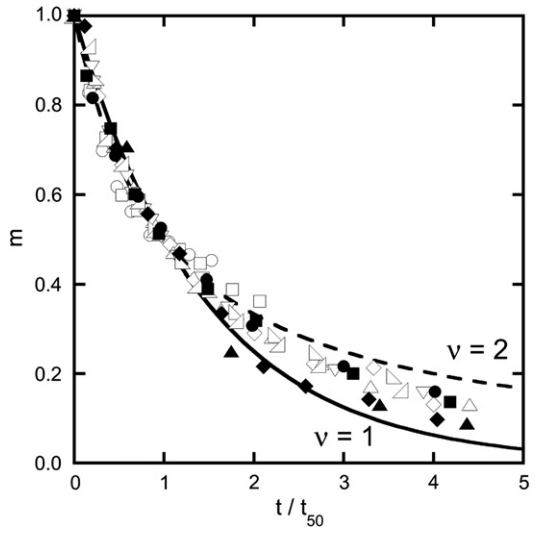

Fig. 1. Monomer fraction versus reduced time for aCgnSH at 50 °C for c_0/[mg mL^{-1}] = 0.6 (○), 0.8 (□), 1.0 (◇), 1.5 (△), 2.1 (▽), 2.9 (◺), and 4.0 (◿), and for aCgnSH at for c_0/[mg mL^{-1}] = 1.2 for T/°C = 51 (●), 52 (■), 53 (◆), and 54 (▲). Error bars are smaller than the size of the symbols.

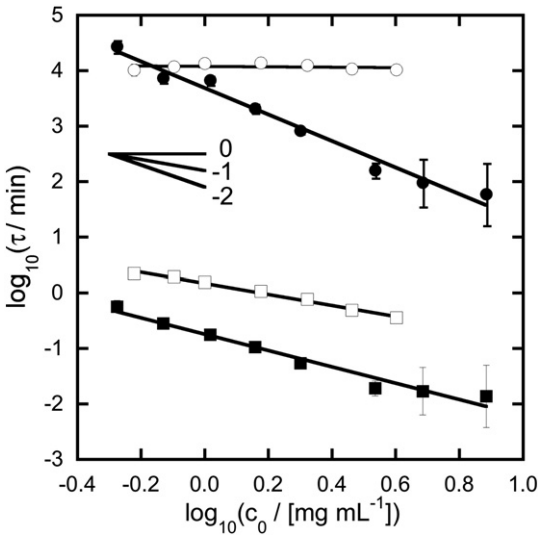

Fig. 3. Rate diagram showing characteristic timescales (inverse rate coefficients) for aCgn nucleation (●) and growth (■), reproduced from ref. [33], and for aCgnSH nucleation (○) and growth (□) as a function of initial protein concentration. Error bars are 95% confidence intervals, and are smaller than the size of the symbols when not visually apparent.

growth by linear chain polymerization [17,22,23]. If aggregate–aggregate condensation steps were kinetically important, M_w/M_0 values would show a pronounced upward curvature when plotted versus $1 - m$, and continue to increase once the supply of monomers had been exhausted [17,21,23,34]. Only linear growth was observed for the conditions tested here for aCgnSH.

Fig. 3 shows the experimentally determined scaling behavior of τ_n and τ_g for aCgn at 65 °C (reproduced from ref. [20]) and for aCgnSH at 50 °C, respectively, using the analysis described in Materials and methods. The results for aCgn are consistent with a nucleus stoichiometry of a mix of trimers and tetramers, and with growth via addition of one monomer per chain polymerization step [18–20]. For aCgnSH, the slope of the least squares fit for τ_g is -1.0 ± 0.1, while that for τ_n is statistically indistinguishable from zero. Combining these values with the scaling behaviors from Eqs. (4a)–(4b) indicate a monomeric nucleus and growth by the addition of monomers for aCgnSH.

That is, growth occurs via a bimolecular process, combining an existing aggregate with a monomer, and therefore the characteristic time scale (akin to a half life) for growth scales as c_0 to the -1 power. However, the characteristic time scale of nucleation is independent of c_0, and this indicates a monomolecular rate-limiting step. The difference in incubation temperatures for the aCgn and aCgnSH measurements was necessary to keep aggregation rates on experimentally tractable time scales, and because incubation times for aCgn to aggregate appreciably at lower temperatures were so long that chemical degradation (hydrolysis/fragmentation, data not shown) became apparent (see also Discussion).

3.3. Aggregate morphology

Values of weight-average molecular weight (M_w) and radius of gyration (R_g) for aCgnSH aggregate populations corresponding to each of the time points ($t > 0$) from Fig. 1 were determined from SEC-MALS. Similar monomer-loss kinetic profiles with corresponding M_w and R_g values

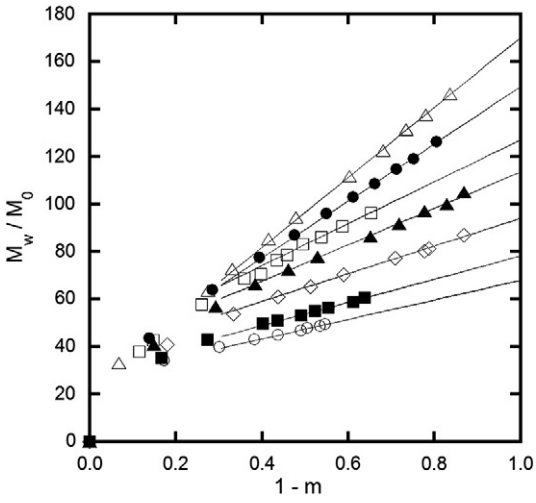

Fig. 2. Reduced aggregate weight-average molecular weight versus aggregate fraction for aCgnSH c_0/[mg mL^{-1}] = 0.6 (○), 0.8 (■), 1.0 (◇), 1.5 (▲), 2.1 (□), 2.9 (●), and 4.0 (△) with incubation at 50 °C. Lines are the corresponding linear least-squares fits to the final five data points for each initial protein concentration. Error bars are smaller than the size of the symbols.

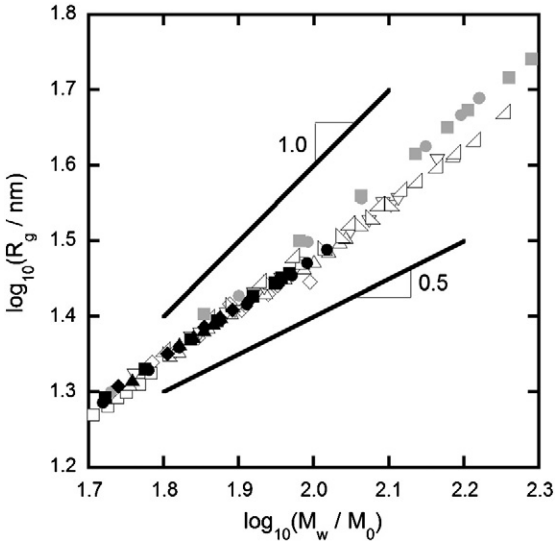

Fig. 4. Scaling of R_g with M_w/M_0 for aCgn at 65 °C for c_0/[mg mL^{-1}] = 0.8 (●), and 1.2 (■), for aCgnSH at 50 °C for c_0/[mg mL^{-1}] = 0.6 (○), 0.8 (□), 1.0 (◇), 1.5 (△), 2.1 (▽), 2.9 (◺), and 4.0 (◿), and for aCgnSH at c_0/[mg mL^{-1}] = 1.2 for T/°C = 51 (●), 52 (■), 53 (◆), and 54 (▲). Solid black lines with slope equal to 1.0 and 0.5 are included as guides to the eye. Error bars are smaller than the size of the symbols.

were generated for aCgn with c_0/[mg mL^{-1}] = 0.8 and 1.2 at 65 °C. Fig. 4 shows the scaling behavior of R_g with reduced weight-average molecular weight (M_w/M_0, with M_0 denoting the molecular weight of the monomer, 25.7 kDa) for both aCgn and aCgnSH aggregates. Linear fits to the data on the log-log scale yielded slopes of 0.79 ± 0.01 and 0.69 ± 0.01 for aCgn and aCgnSH, respectively. Reported uncertainties are 95% confidence intervals from the statistical uncertainties of the regression. These results agree quantitatively with previous data for aCgn aggregates determined from batch static light scattering [20], and indicate the morphology of aggregates for aCgn and aCgnSH is that of a semi-flexible, unbranched polymer. Representative TEM images of aCgn and aCgnSH aggregates (Fig. 5) also show that the aggregates are linear polymers, with no evidence of significant branching or coalescence of the aggregates. The aggregates of aCgnSH are somewhat shorter than those for aCgn, but otherwise are very similar in morphology.

3.4. Cross-seeding

Aggregates of aCgn were previously shown to act as seeds for unaggregated aCgn monomer, in that addition of preformed aggregates to monomeric aCgn caused large increases in the rate of monomer loss at the elevated temperatures needed to populate molten globule aCgn monomers [18]. Results summarized in the Supporting Material show that aCgn aggregates can act as "seeds" for consuming aCgn monomers, and vice versa. Illustrative TEM images of aggregates from seeding experiments are shown in panels C through F of Fig. 5, and indicate no significant change in morphology compared to aggregates that were freshly formed from parent monomer solutions.

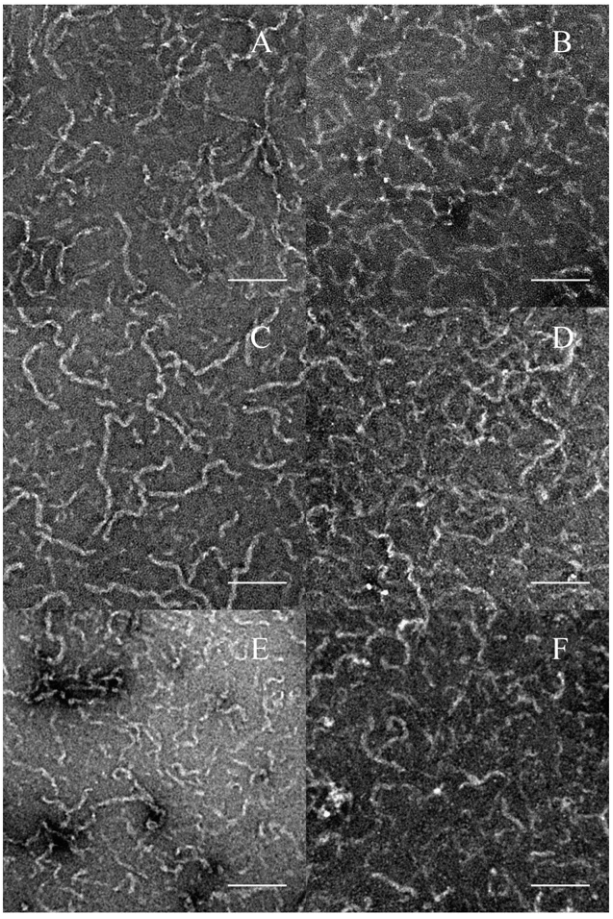

Fig. 5. Electron micrographs of (A) aCgn aggregates from 65 deg. C for 1 h; (B) aCgnSH aggregates from 50° C for 10 h; (C) cross-seeded aCgnSH monomers with aCgn aggregates, with incubation at the same conditions as in panel B; (D) cross-seeding of aCgn monomers with aCgnSH aggregates, with incubation at the same conditions as in panel A; (E) aCgn aggregates from panel A after additional incubation under the conditions for panel C; (F) aCgnSH aggregates from panel B after additional incubation at the conditions of panel D. See also main text for additional details. Scale bars are 200 nm for each pane.

3.5. Circular dichroism and intrinsic fluorescence

The main panel of Fig. 6 shows the mean residue ellipticity ([θ]) at 20 °C as a function of wavelength for native monomer, unfolded monomer in 6 M urea, and aggregates for aCgn and aCgnSH, respectively. Corresponding equilibrium intrinsic fluorescence spectra are shown in the inset. In all cases, aCgn and aCgnSH spectra are statistically indistinguishable for each of the native, unfolded, and aggregate states. The interference from urea precludes collection of accurate CD spectra below approximately 220 nm for the unfolded states, which is a common limitation when considering protein CD spectra in the presence of denaturing concentrations of urea [19,35]. For folded monomers, the shape of the CD spectra are unusual, in that they do not show a clear minimum ~212 nm for a purely beta-sheet protein, or the double minima at ~208 nm and ~222 nm for a purely alpha-helical protein; inspection of the X-ray crystal structure for aCgn indicates that it contains relatively large regions of non-helix and non-sheet structure, presumably held intact by the multiple disulfide bonds that persist in both aCgn and aCgnSH [20].

Aggregate CD spectra indicate increased β-sheet secondary structure, and are distinct from both native and unfolded spectra. Aggregate and unfolded fluorescence spectra are red-shifted relative to the native state, with increased intensity. In all cases, measurements of aCgn monomer and aggregate secondary and tertiary structure are consistent with those reported earlier [19,20]. Further, extrinsic fluorescence spectra from thioflavine T binding to nonnative aggregates of aCgn and aCgnSH are essentially indistinguishable (see Supporting Information).

3.6. Urea unfolding/refolding

aCgnSH urea unfolding/refolding measurements were performed and monitored with intrinsic fluorescence at 20 °C and 30 °C. Significantly higher temperatures, approaching those in Fig. 1, were not practical because aCgnSH aggregates readily on the multi-hour time scales of sample preparation for equilibrium or for stopped-flow unfolding/refolding (data not shown), similar to the behavior of aCgn [19]. Fig. 7 shows representative unfolding/refolding COM^{-1} data for aCgnSH

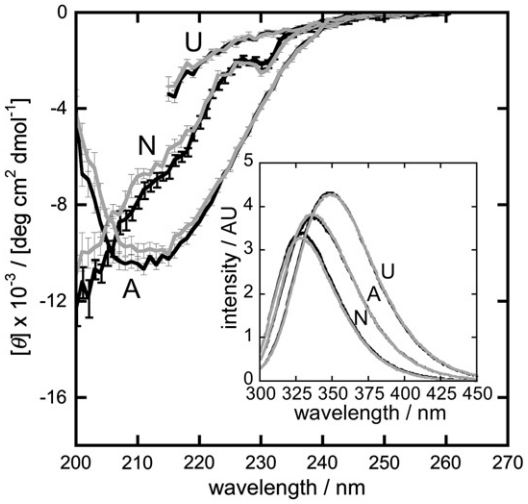

Fig. 6. (*main panel*) CD spectra at 20 °C for native monomer, (N), unfolded monomer in 6 M urea, (U), and aggregate, (A), for aCgn (solid black) and aCgnSH (solid gray), respectively. Error bars are 95% confidence intervals. (*inset*) Fluorescence emission spectra at 20 °C for native monomer, (N), unfolded monomer in 6 M urea, (U), and aggregate, (A), for aCgn (solid black) and aCgnSH (solid gray), respectively.

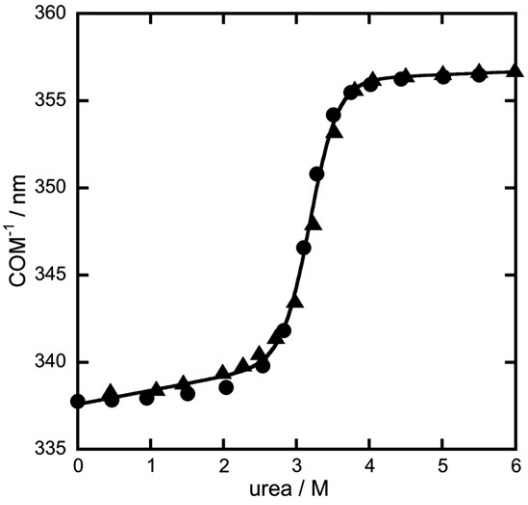

Fig. 7. Fluorescence COM^{-1} values as a function of urea concentration at 20 °C for aCgnSH monomer unfolding (●) and refolding (♦). The line is the corresponding fit to the two-state unfolding model. Error bars are smaller than the size of the symbols.

at 20 °C. Measurements at 30 °C yielded qualitatively similar curves (not shown). Unfolding and refolding data were combined and globally regressed against a two-state model using a nonlinear least squares method implemented in MATLAB® (MathWorks, Natick, MA), as in ref. [19]. Values for ΔG^0_{unf} obtained from the combined global regression did not differ within statistical uncertainty from values obtained by fitting unfolding and refolding data separately.

The fitted value for ΔG^0_{unf} for aCgnSH at 20 °C is 9.7 ± 0.7 kcal mol^{-1}, while that for 30 °C is 8.5 ± 0.6 kcal mol^{-1}. The value at 30 °C for aCgn [19] is 9.2 ± 0.5 kcal mol^{-1} The results show no difference in unfolding free energy, within statistical uncertainty. Therefore, if removing the C191-C220 disulfide bond does result in a change in unfolding free energy, it is not large enough to be detected with this technique [36]. As DSC was convoluted with aggregation, it was also not possible to reliably answer this question with that technique. Although previous work has shown that removing a single disulfide can result in reduced ΔG_{unf} values, in the present case this may be mitigated by the fact that four out of five native disulfides remain intact. Similarly, those remaining disulfides are anticipated to help prevent significant differences in the measurable secondary or tertiary structure for aCgn and aCgnSH monomers in Fig. 6, despite the potential increased loop entropy that one might anticipate would be liberated by the removal of a disulfide bond if other disulfides were not present.

4. Discussion

The average aggregate structure and morphology were probed with a combination of scattering and spectroscopic data for monomers and aggregates of aCgn and aCgnSH. Fig. 4 shows the scaling behavior of aggregate radius of gyration (R_g) with reduced weight average molecular weight (M_w/M_0), along with negatively stained transmission electron micrographs in Fig. 5. The magnitude of the scaling exponent, or the slope of the data in Fig. 4, is related to the underlying morphology of the aggregates, where values of 0.5 and 1.0 represent the Gaussian chain and rigid rod limits, respectively [37]. All of the data for aCgnSH fall on a common curve, regardless of initial protein concentration or incubation temperature, indicating that the underlying morphology of the aggregates is well-conserved as a semi-flexible linear polymer.

While there is a quantitative difference in the scaling exponents for aCgn and aCgnSH aggregates, this difference is relatively small and indicates that reducing the C191-C220 disulfide yields aggregates that are still linear, semi-flexible chains. This conclusion is also consistent with the TEM results in Fig. 5. The filaments are similar in that they are unbranched and do not appear to be significantly bundled with one another. Although the average diameters of the filaments are slightly different, this is well within the standard deviation of those values (not shown). As noted above, the morphology does not appear to depend on whether aggregates are prepared with or without cross-seeding between aCgn and aCgnSH species.

Far-UV CD and intrinsic fluorescence spectroscopy (Fig. 6) show that the overall structural differences between monomers and aggregates of aCgn and aCgnSH are subtle, at least as detected by far-UV CD and solvent exposure of aromatic amino acids via intrinsic fluorescence. The CD spectra of the native, unfolded, and aggregate states for both the wild-type and the partially reduced protein are identical within the confidence limits of the measurement.

This indicates that breaking the C191-C220 disulfide leaves the global secondary and tertiary structure of native aCgn largely intact, and this is perhaps not unexpected considering that four disulfides remain intact in the molecule. A similar observation was also made for a different serine protease, in which the crystal structure was determined for both the wild-type protein and its Ala mutant with the analogous disulfide removed [38], but in that case the loss of the disulfide impacted the catalytic activity of thrombin. aCgn is not catalytically active itself, as it is the zymogen of the serine protease chymotrypsin. This observation does not preclude the possibility of important local conformational rearrangements in the vicinity of the reduced disulfide that the bulk spectroscopic measurements may be unable to detect. ThT binding (see Supporting information) is also indistinguishable between the aggregates of aCgn and aCgnSH, with no appreciable binding to monomeric protein. In addition, fiber X-ray diffraction measurements for aCgnSH aggregates show the canonical cross-beta pattern (Supporting information), as found previously for aCgn aggregates under these solvent conditions [39]. In addition, aggregates of aCgn can "seed" aggregation of aCgnSH, and vice versa. Together, these results show that aggregates of aCgnSH therefore appear to retain the basic amyloid structure associated with aggregates of aCgn.

Despite the similarities in morphology and structure of the aggregates for aCgn and aCgnSH, reducing the native C191-C220 disulfide bond in aCgn results in a fundamental change in the underlying mechanism of nonnative aggregation. This is evidenced by the large reduction in nucleus size (cf. Fig. 3), while growth appears to be qualitatively and semi-quantitatively the same for aCgn and aCgnSH. This is summarized schematically in Scheme 1. Unfolding is required both for aCgn and aCgnSH to aggregate. For aCgn, these reactive unfolded species reversibly self-associate until an irreversible step converts the reversible oligomer of unfolded molecules into the smallest irreversible aggregate. This nucleus then grows by the subsequent addition of monomers. For aCgnSH, there are no reversible oligomerization steps, and the unfolded monomer converts directly (irreversibly) into a monomeric nucleus — i.e., a structurally distorted monomer is able to form a sufficiently stable "template" to recruit other unfolded monomers at a growth rate ($\sim 1/\tau_g$) that is orders of magnitude faster than the nucleation rate ($\sim 1/\tau_n$). The present data provides no direct structural evidence to indicate gross morphological or three-dimensional structural changes between the unfolded aCgn and unfolded aCgnSH monomers. However, one can speculate that removal of the disulfide bond provides more structural flexibility to allow exposure of aggregation-prone "hot-spot sequences" in the aCgnSH monomer, and that conformational transition becomes rate-limiting for recruiting a neighboring aCgnSH protein chain to initiate aggregation.

Previous stopped-flow kinetic unfolded/refolding measurements with aCgn at much lower temperatures showed that the time scales for folding/unfolding are orders of magnitude faster than those for aggregation, and that folding/unfolding was 2-state with no discernable folding/unfolding intermediates, consistent with a clear isobestic point in the equilibrium unfolding FL spectra as a function of urea concentration [19]. While stopped-flow measurements were beyond the scope of this study, the equilibrium FL measurements for aCgnSH also showed an

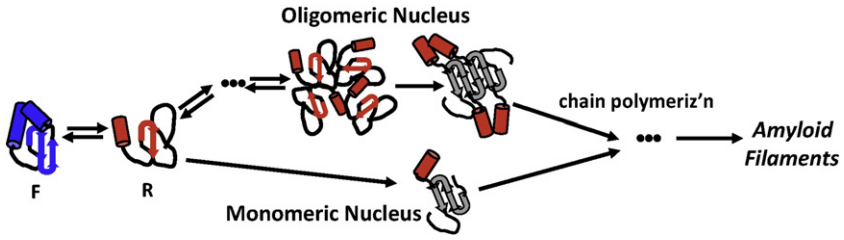

Scheme 1. Alternative nucleation pathways for aCgn (oligomeric nucleus) and aCgnSH (monomeric nucleus) for amyloid formation.

isobestic point. Ideally, stopped-flow experiments at high temperatures (~50 °C) would be desirable to directly measure the unfolding rate coefficient and compare it to that for nucleation of aCgnSH aggregates. Preliminary data (not shown) from SEC-MALS indicate that aggregates formed too quickly, during sample preparation and hold times for stopped-flow measurements, to allow unfolding to measured directly at the conditions where aggregation kinetics were quantified.

A monomeric nucleus, while somewhat counterintuitive, has also been implied for other systems [40,41]. However, in one case that conclusion has been called into question [42], based at least in part because the earlier analysis and experiments did not incorporate details of the aggregate size distribution and growth kinetics. The results here do not suffer from those limitations, and are consistent with a reduction of nucleus size for aCgnSH, compared to the trimer and larger oligomers implicated as nuclei for aCgn. This suggests that elimination of the C191-C220 disulfide bond greatly reduces one or more key barriers for creating stable aggregates for aCgn.

A monomeric nucleus is consistent with unfolding as the rate-limiting step for nucleation [3,41], which indicates a dramatic reduction in the nucleation barrier(s) for aggregation. This presumably occurs because of the greater freedom of the unfolded monomer to explore conformational space so as to find the amyloid template structure that readily recruits additional monomers to add so easily to it — i.e., time scale for growth after the nucleated structure is formed is ~2–3 orders of magnitude faster than nucleation, depending on the initial protein concentration (cf. Fig. 3).

Finally, aggregates of aCgn have been previously shown to dissociate completely in high concentrations of urea [19,43]. Using SEC-MALS, aggregates composed of aCgnSH were empirically found to not be dissociable up to 8 M urea over multi-day time scales (data not shown). Therefore, although the aggregate structures were sufficiently similar to allow monomers of the other species to cross-aggregate, this result suggests that there is some degree of structural difference that was not discernable via any of the spectroscopic, scattering, or microscopy techniques available here. This is possibly a local structural rearrangement within the amyloid core of the molecule [39], or alternatively perhaps disulfide cross-links between aCgnSH chains in the aggregates occurred over time. The current results remain inconclusive regarding this question, but preliminary data from incubating aCgnSH aggregates at extreme pressure (~kilobars) showed some but not complete (~30%) monomer recovery (data not shown), which argues against the latter. Future work will focus on answering this question with the aid of higher resolution structural techniques.

5. Summary and conclusions

The aggregation mechanism and morphology/structure of a partially reduced form of aCgn were characterized under solution conditions where aggregation proceeds through a nucleation + chain polymerization mechanism. The underlying secondary structure, ThT binding, and exposure of fluorophores in the folded, unfolded, and aggregated states for aCgn and aCgnSH were indistinguishable within experimental uncertainty. In addition, aCgn and aCgnSH both formed amyloid filaments with similar morphology, and each was able to cross-seed with the monomers of the other species.

The main difference between the aggregation behavior of aCgn and aCgnSH was a much smaller nucleus size (stoichiometry), which was inferred to indicate a reduction in the conformational barrier(s) to nucleation. This suggests that disulfides in wild type aCgn may impede or slow the kinetics of forming a stable nucleus/structural "template" for amyloid of aCgn. That is, for the WT molecule a stable nucleus requires multiple proteins to simultaneously "find" the amyloid structure. For aCgnSH, even a monomer can easily "find" that structure through a conformational search, and provide it as a structural template for recruiting other monomers as part of growth. This is consistent with the mechanism for aCgn, as nucleation was previously shown to involve a significant entropic bottleneck [18], presumably involving a difficult conformational search.

More generally, the results here provide additional motivation for considering the role of S – S bonds in ameliorating non-native aggregation by providing conformational barriers to nucleation itself, in addition to any improvements in monomer unfolding free energies that may also be realized.

Acknowledgments

The authors thank A. S. Robinson for use of the fluorimeter, and the staff at the Advanced Photon Source beamline 4-ID-E. CJR gratefully acknowledges support, in part, from the National Institutes of Health (R01 EB006006, P20 RR015588).

Appendix A. Supplementary data

Supplementary data to this article can be found online at http://dx.doi.org/10.1016/j.bpc.2013.11.005.

References

[1] C.M. Dobson, Principles of protein folding, misfolding and aggregation, Semin. Cell Dev. Biol. 15 (2004) 3–16.
[2] C.J. Roberts, Non-native protein aggregation kinetics, Biotechnol. Bioeng. 98 (2007) 927–938.
[3] W.F. Weiss IV, T.M. Young, C.J. Roberts, Principles, approaches, and challenges for predicting protein aggregation rates and shelf life, J. Pharm. Sci. 98 (2009) 1246–1277.
[4] A.L. Fink, Protein aggregation: folding aggregates, inclusion bodies and amyloid, Fold. Des. 3 (1998) R9–R23.
[5] E.Y. Chi, S. Krishnan, T.W. Randolph, J.F. Carpenter, Physical stability of proteins in aqueous solution: mechanism and driving forces in nonnative protein aggregation, Pharm. Res. 20 (2003) 1325–1336.
[6] W. Wang, Protein aggregation and its inhibition in biopharmaceutics, Int. J. Pharm. 289 (2005) 1–30.
[7] H. Schellekens, Bioequivalence and the immunogenicity of biopharmaceuticals, Nat. Rev. Drug Discov. 1 (2002) 457–462.
[8] V.S. Purohit, C.R. Middaugh, S.V. Balasubramanian, Influence of aggregation on immunogenicity of recombinant human Factor VIII in hemophilia A mice, J. Pharm. Sci. 95 (2006) 358–371.
[9] A.S. Rosenberg, Effects of protein aggregates: an immunologic perspective, AAPS J. 8 (2006) E501–E507.
[10] D. Eisenberg, R. Nelson, M.R. Sawaya, M. Balbirnie, S. Sambashivan, M.I. Ivanova, et al., The structural biology of protein aggregation diseases: fundamental questions and some answers, Acc. Chem. Res. 39 (2006) 568–575.
[11] C.M. Dobson, Protein aggregation and its consequences for human disease, Protein Pept. Lett. 13 (2006) 219–227.
[12] S.L. Flaugh, I.A. Mills, J. King, Glutamine deamidation destabilizes human gammaD-crystallin and lowers the kinetic barrier to unfolding, J. Biol. Chem. 281 (2006) 30782–30793.

[13] S.W. Snyder, U.S. Ladror, W.S. Wade, G.T. Wang, L.W. Barrett, E.D. Matayoshi, et al., Amyloid-beta aggregation: selective inhibition of aggregation in mixtures of amyloid with different chain lengths, Biophys. J. 67 (1994) 1216–1228.
[14] M.S. Ricci, M.M. Pallito, L.O. Narhi, T. Boone, D.N. Brems, Mutational approach to improve physical stability of protein therapeutics susceptible to aggregation: role of altered conformation in irreversible precipitation, in: R.M. Murphy, A.M. Tsai (Eds.), Misbehaving Proteins Protein MisFolding Aggreg. Stab, Springer, New York, NY, 2006.
[15] E. Sahin, J.L. Jordan, M.L. Spatara, A. Naranjo, J.A. Costanzo, W.F. Weiss, et al., Computational design and biophysical characterization of aggregation-resistant point mutations for γD crystallin illustrate a balance of conformational stability and intrinsic aggregation propensity, Biochemistry (Mosc) 50 (2011) 628–639.
[16] J.W. Kelly, Alternative conformations of amyloidogenic proteins govern their behavior, Curr. Opin. Struct. Biol. 6 (1996) 11–17.
[17] Y. Li, W.F. Weiss, C.J. Roberts, Characterization of high-molecular-weight nonnative aggregates and aggregation kinetics by size exclusion chromatography with inline multi-angle laser light scattering, J. Pharm. Sci. 98 (2009) 3997–4016.
[18] J.M. Andrews, C.J. Roberts Weiss, Nucleation, growth, and activation energies for seeded and unseeded aggregation of α-chymotrypsinogen A†, Biochemistry (Mosc) 47 (2008) 2397–2403.
[19] J.M. Andrews, C.J. Roberts, Non-native aggregation of α-chymotrypsinogen occurs through nucleation and growth with competing nucleus sizes and negative activation energies†, Biochemistry (Mosc) 46 (2007) 7558–7571.
[20] W.F. Weiss IV, T.K. Hodgdon, E.W. Kaler, A.M. Lenhoff, C.J. Roberts, Nonnative protein polymers: structure, morphology, and relation to nucleation and growth, Biophys. J. 93 (2007) 4392–4403.
[21] Y. Li, B.A. Ogunnaike, C.J. Roberts, Multi-variate approach to global protein aggregation behavior and kinetics: effects of pH, NaCl, and temperature for α-chymotrypsinogen A, J. Pharm. Sci. 99 (2010) 645–662.
[22] J.M. Andrews, C.J. Roberts, A Lumry–Eyring nucleated polymerization model of protein aggregation kinetics: 1. Aggregation with pre-equilibrated unfolding, J. Phys. Chem. B 111 (2007) 7897–7913.
[23] Y. Li, C.J. Roberts, Lumry–Eyring nucleated-polymerization model of protein aggregation kinetics. 2. Competing growth via condensation and chain polymerization, J. Phys. Chem. B 113 (2009) 7020–7032.
[24] G.L. Ellman, Tissue sulfydryl groups, Arch. Biochem. Biophys. 82 (1959) 70–77.
[25] P.W. Riddles, R.L. Blakeley, B. Zerner, Ellman's reagent: 5,5′-dithiobis(2-nitrobenzoic acid)—a reexamination, Anal. Biochem. 94 (1979) 75–81.
[26] T.E. Creighton, Disulphide bonds between cysteine residues, Protein Struct. Pr. Approach, 1st ed., Oxford University Press, Oxford, 1989.
[27] M. Smith, Peptides and proteins, in: H. Sober (Ed.), Handb. Biochem, The Chemical Rubber Co., Cleveland, OH, 1970, pp. 71–98.
[28] E. Sahin, C.J. Roberts, Size-exclusion chromatography with multi-angle light scattering for elucidating protein aggregation mechanisms, Methods Mol. Biol. Clifton NJ 899 (2012) 403–423.
[29] K. Kawahara, C. Tanford, Viscosity and density of aqueous solutions of urea and guanidine hydrochloride, J. Biol. Chem. 241 (1966) 3228–3232.
[30] Z. Shaked, R.P. Szajewski, G.M. Whitesides, Rates of thiol-disulfide interchange reactions involving proteins and kinetic measurements of thiol pKa values, Biochemistry (Mosc) 19 (1980) 4156–4166.
[31] J. Houk, R. Singh, G.M. Whitesides, Measurement of thiol-disulfide interchange reactions and thiol pKa values, in: O.W.G. William, B. Jakoby (Eds.), Methods Enzymol, Academic Press, 1987, pp. 129–140.
[32] C.N. Pace, G.R. Grimsley, J.A. Thomson, B.J. Barnett, Conformational stability and activity of ribonuclease T1 with zero, one, and two intact disulfide bonds, J. Biol. Chem. 263 (1988) 11820–11825.
[33] D.L. Sondack, A. Light, Comparative studies on the modification of specific disulfide bonds of trypsinogen and chymotrypsinogen, J. Biol. Chem. 246 (1971) 1630–1637.
[34] R.K. Brummitt, D.P. Nesta, L. Chang, A.M. Kroetsch, C.J. Roberts, Nonnative aggregation of an IgG1 antibody in acidic conditions, part 2: nucleation and growth kinetics with competing growth mechanisms, J. Pharm. Sci. 100 (2011) 2104–2119.
[35] T.V. Chalikian, J. Völker, D. Anafi, K.J. Breslauer, The native and the heat-induced denatured states of alpha-chymotrypsinogen A: thermodynamic and spectroscopic studies, J. Mol. Biol. 274 (1997) 237–252.
[36] J.M. Scholtz, G.R. Grimsley, C.N. Pace, Solvent denaturation of proteins and interpretations of the m value, Methods Enzymol. 466 (2009) 549–565.
[37] W. Burchard, Solution properties of branched macromolecules, in: J. Roovers (Ed.), Branched Polym. II, Springer, New York, NY, 1999, pp. 113–194.
[38] L.A. Bush-Pelc, F. Marino, Z. Chen, A.O. Pineda, F.S. Mathews, E. Di Cera, Important role of the cys-191 cys-220 disulfide bond in thrombin function and allostery, J. Biol. Chem. 282 (2007) 27165–27170.
[39] A. Zhang, J.L. Jordan, M.I. Ivanova, W.F. Weiss, C.J. Roberts, E.J. Fernandez, Molecular level insights into thermally induced α-chymotrypsinogen A amyloid aggregation mechanism and semiflexible protofibril morphology, Biochemistry (Mosc) 49 (2010) 10553–10564.
[40] S. Chen, F.A. Ferrone, R. Wetzel, Huntington's disease age-of-onset linked to polyglutamine aggregation nucleation, Proc. Natl. Acad. Sci. U. S. A. 99 (2002) 11884–11889.
[41] Z. Ignatova, L.M. Gierasch, Aggregation of a slow-folding mutant of a beta-clam protein proceeds through a monomeric nucleus, Biochemistry (Mosc) 44 (2005) 7266–7274.
[42] C.C. Lee, R.H. Walters, R.M. Murphy, Reconsidering the mechanism of polyglutamine peptide aggregation, Biochemistry (Mosc) 46 (2007) 12810–12820.
[43] R.K. Brummitt, J.M. Andrews, J.L. Jordan, E.J. Fernandez, C.J. Roberts, Thermodynamics of amyloid dissociation provide insights into aggregate stability regimes, Biophys. Chem. 168–169 (2012) 10–18.